

# Sign and relevance learning

Sama Daryanavard<sup>1</sup> and Bernd Porr<sup>1</sup>

## Abstract

Standard models of biologically realistic, or inspired, reinforcement learning employ a global error signal which implies shallow networks. However, on the other hand, local learning rules allow networks with multiple layers. Here, we present a network combining local learning with global modulation where neuromodulation controls the amount of plasticity change in the whole network, while the sign of the error is passed via a bottom-up pathway through the network. Neuromodulation can be understood as a rectified error, or relevance, signal while the bottom-up sign of the error signal decides between long-term potentiation and long-term depression. We demonstrate the performance of this paradigm with a real robotic task as a proof of concept.

## Keywords

neuromodulation, reinforcement learning, deep learning, synaptic plasticity, dopamine, serotonin

## Introduction

The learning of an organism is understood in the context of interactions with its environment facilitated through sensory inputs and motor outputs which, in turn, cause new sensory inputs (Maffei et al. 2017). The framework for such learning is closed-loop learning (von Uexküll 1926) where actions lead to either negative or positive consequences; this is the realm of reinforcement learning (Dayan and Balleine 2002). Central to reinforcement learning in a biologically realistic framework is the reward prediction error. In the 90s, Schultz et al. (1997) suggested that dopamine codes this error (Bromberg-Martin et al. 2010; Wood et al. 2017; Takahashi et al. 2017) which is reminiscent of the so-called temporal difference error in machine learning (Sutton 1988). This led to the assumption that the brain resembles an actor/critic architecture where dopamine, as the reward prediction error, drives synaptic changes in the striatum (Humphries et al. 2006). Another interpretation of the actor/critic architecture is a nested closed-loop platform where an inner reflex loop generates an error signal which tunes an actor in an outer loop to create anticipatory actions, in other words, the actor generates a forward model of the reflex (Porr and Wörgötter 2002). Thus the actor/critic architecture can be used for both model-based (Verschure and Coolen 1991) and model-free learning.

However, using just a global error signal such as the dopamine reward prediction error has its limitations as the error signal affects all neurons (Humphries et al. 2006; O'Reilly and Frank 2006) and thus multi-layer networks have limited usefulness. Indeed, the standard models of decision-making focus on the striatum which is a single-layer decision network innervated by dopamine and receives its input from the cortex (Humphries et al. 2006) which itself is not involved in decision-making but is only used for working memory operations and signal conditioning (O'Reilly and Frank 2006).

Cortical networks, such as the orbitofrontal and medial prefrontal cortices, are also heavily involved in reinforcement learning (Haber et al. 1995; Berthoud 2004;

Rolls and Grabenhorst 2008). In particular in the context of cortical pyramidal neurons one should not forget that the main method by which plasticity is induced is via local learning rules such as Hebbian learning (Hebb 1949; Bliss and Lomo 1973) or spike-timing-dependent plasticity (STDP) (Markram et al. 1997) with its underlying post-synaptic calcium dynamics where a strong concentration causes long-term potentiation (LTP) and a small concentration causes long-term depression (LTD) (Lu et al. 2001; Castellani et al. 2001). These are local learning rules, and they interact with the global neuromodulator (Mattson et al. 2004; Lovinger 2010), in particular serotonin, (Roberts 2011; Linley et al. 2013) which appears to be a rectified reward prediction error or reward anticipation controlling the level of plasticity (Luo et al. 2015; Li et al. 2016). From a theoretical point of view, this inspired ISO3 learning where differential Hebb is combined with a rectified error signal which is called "relevance". However, also this network is shallow having just one layer.

In this paper, we present a novel learning mechanism which takes the single-layer approach of ISO3 learning (Porr and Wörgötter 2007), namely having both local and global neuromodulator-controlled plasticity whilst expanding it to networks which multiple layers. Our network employs a bottom-up pass of the *sign* of an error signal, deciding upon LTP or LTD, while a global neuromodulator controls the speed of learning. As a proof of concept, we employ a simple line-following task deployed on a real robot whose deviation generates an error signal used to train the network.

<sup>1</sup>Biomedical Engineering Division, School of Engineering, University of Glasgow, Glasgow G12 8QQ, UK.

## Corresponding author:

Sama Daryanavard, University of Glasgow, Glasgow G12 8QQ, UK.  
Email: s.daryanavard.1@research.gla.ac.uk

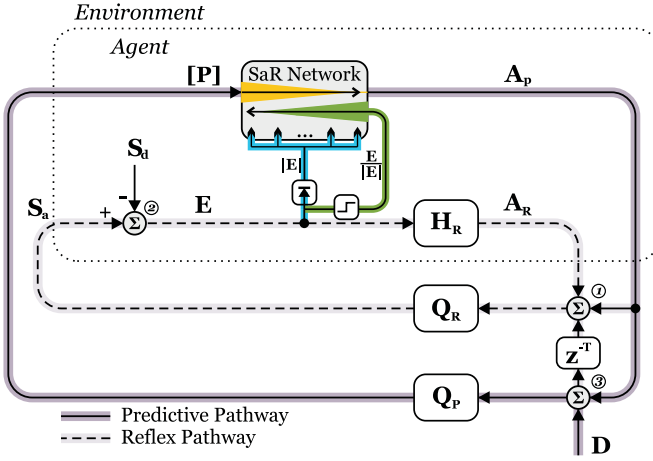


**Figure 1.** SaR learning platform. The boundary between the agent and the environment is marked with a dotted rectangle. The platform consists of two loops: the inner reflex loop, shown with dashed lines, and the outer predictive (or learning) loop, shown with solid lines.

## The sign and relevance (SaR) learning platform

The sign and relevance (SaR) learning platform is presented in Figure 1. The reflex mechanism, the learning pathway and the flow of signals are described below.

### The reflex loop

Reflex is one of the most innate drivers of an organism’s behaviour. It is a triggered involuntary action that is carried out without prior knowledge of the stimuli. A reflex often serves to ensure the survival and success of the agent. In this work, the agent is a navigational robot that aims to follow a path. When encountering a bend in the path, this innate reflex mechanism provides the organism with an immediate reaction that is designed to recover from the disturbance. Therefore, a reflex is a fixed closed-loop controller that opposes collective disturbances with maintaining its desired state.

When the disturbance  $D$  passes through the reflex environment  $Q_R$  (refer to Figure 1), it causes a new state for the agent. This actual state  $S_a$  is compared to the desired state  $S_d$  at node ②. The difference between the two states is realised by the agent’s sensors, this discrepancy generates an error signal termed the control error ( $E$ ):

$$E = S_d - S_a \quad (1)$$

This drives the reflex mechanism  $H_R$  to take an action  $A_R$  which, by design, corrects for the disturbance and resumes equilibrium at node ①; this summarises the reflex pathway. Although this loop combats the disturbances by design, it is incapable of disturbance avoidance. To maintain the desired state at all times, the reflex loop is enclosed within the outer predictive loop whose task is to combat the disturbance  $D$  before it reaches the reflex loop.

### The predictive loop

In contrast to the reflex, the sign and relevance (SaR) network acts in anticipation, and with prior knowledge, of

the disturbance. This is possible because the environment is structured in a way that the disturbance  $D$  delayed by  $z^T$  time-steps so that the learner can generate anticipatory actions. The learner aims to interact with the environment and meet the objective, without invoking the reflex mechanism. In this work, the learner aims to follow the path without making use of the reflex sensors.

The disturbance is first received by the learner’s environment  $Q_P$  and is translated into predictive sensory inputs  $[P]$ . Based on this input information, the network generates a predictive action  $A_P$  in an attempt to resume, or preserve, system equilibrium at node ①, where the effects of  $A_P$ , the delayed  $D$  and the reflex action  $A_R$  are combined before travelling through to the reflex loop. If successful,  $A_P$  fends off the delayed  $D$  precisely to yield zero at this summation node\* and thus, the reflex loop is not evoked. If unsuccessful, however, the summation yields a non-zero signal which is received by  $Q_R$ ; this evokes the reflex loop and leads to a non-zero control error signal.

### The control error ( $E$ )

The function of control error is two-fold: 1) it is received by the reflex  $H_R$  to generate the reflex action  $A_R$ , as described above, and 2) it serves as instructive feedback for the learner. Through iterations, the non-zero  $E$  signal tunes the internal parameters of the SaR network. The learning terminates when  $A_P$  fends off the disturbance at node ③ precisely and persistently. In this case, the reflex loop is no longer evoked,  $E$  remains at zero, and the learner undergoes no further changes. Thus, the SaR network will have successfully generated the forward model of the reflex, similarly to the model-based learning paradigms presented in the work by [Porr and Wörgötter \(2002, 2006, 2003\)](#).

### The SaR learner

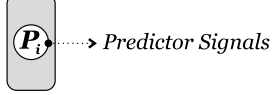
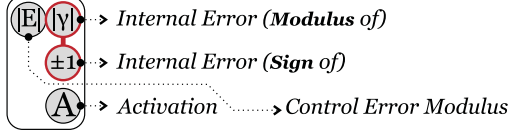
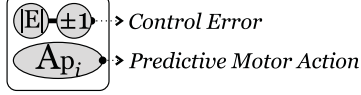
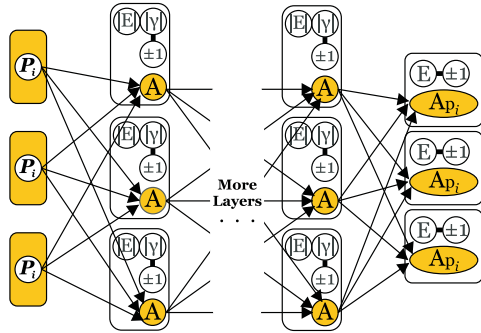
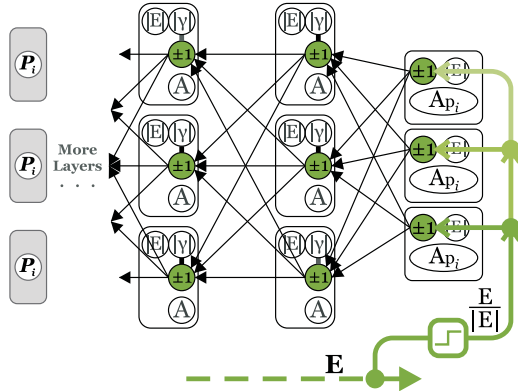
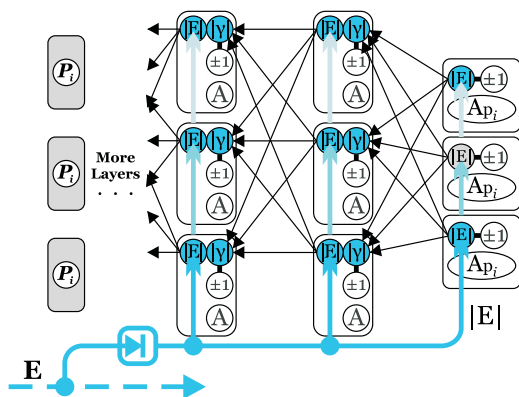
The learner generates the forward model of the reflex through the mapping of its predictive actions onto a set of sensory consequences which is realised by the agent — the control error signal. The unique property of the SaR paradigm is that the instructive feedback of  $E$  is facilitated through two distinct pathways: 1) the bottom-up pass of the *sign* of  $E$  (green traces), and 2) global intervention of the rectified  $E$  (blue traces); refer to Figure 1.

Figure 2 illustrates these pathways in detail. The symbols used for each neuron type are introduced in Panel 2A, these are neurons in the input, hidden and output layers. The input neurons receive the predictive signal to be injected into the network. The hidden layers contain the control error, their internal error (sign and modulus of), and their activation. At last, the output neurons contain the control error and the final predictive motor action of the network.

The SaR learner employs a conventional feed-forward neural network with fully-connected layers. Panel 2B shows the forward pass of signals in the network, from the predictive inputs  $P_i$ , to activations  $A$  in hidden layers, and predictive outputs  $A_{pi}$  in the output layer.

Panel 2C shows the bottom-up pass of the sign of the error  $E$ . The green traces mark the entry of the error  $E$  from the

\*note that  $A_R$  is zero at this instance.

**A) Neuron types:****1) Input neuron type****2) Hidden neuron type:****3) Output neuron type:****B) Top-down pass of activations****C) Bottom-up pass of sign of E****D) Local pass of modulus of E**

**Figure 2.** Signal pathways within SaR network: A) Symbol introduction: 1) an input neuron, 2) a hidden neuron, and 3) an output neuron. B) The top-down pass of predictive signals, calculation of activations, and formation of motor commands. C) The bottom-up pass of the sign of  $E$ . D) The local pass of  $E$ .

reflex loop onto the output neurons. The sign of the error  $E$  is passed from the final layer to the deeper layers. Within each layer, the sign of the resulting value is passed to the deeper layers. This results in an error of  $\pm 1$  within each neuron which primes their connections to be strengthened ( $+1$ ) or weakened ( $-1$ ). This is analogous to LTP and LTD in the context of neurophysiology.

Panel 2D shows the local pass of the modulus of  $E$ . The blue traces show the entry of this signal from the closed-loop platform onto every layer. This value innervates each neuron and is passed to their adjacent deeper neurons only. The absolute value of the resulting sum dictates the amount by which the previously primed connections are strengthened or weakened. This is analogous to the effect of neuromodulators on plasticity, in particular serotonin.

## Mathematical derivation of sign and relevance (SaR) learning

In this section, we derive the learning rule for sign and relevance (SaR) paradigm. First, top-down pass of predictive inputs is derived, according to the conventional flow of signals in fully-connected feed-forward neural networks. Next, a mathematical expression of the learning goal in its general sense is presented, where a differentiable function is optimised through adjustments of weights. Subsequently, this learning goal is unravelled with regards to the close-loop platform as well as the inner working of the neural network. With that, the learning rule for a conventional gradient descent method (GDM) is derived which leads to the formulation of the SaR update rule.

### Top-down pass of activations

Figure 3 demonstrates the inner components of neurons and their connections. The top-down pass of activations, from  $j^{th}$  neuron in  $\ell^{th}$  layer,  $\mathcal{n}_j^\ell$ , to all neurons in the adjacent deeper layer,  $\mathcal{n}_{0 \rightarrow K}^{\ell+1}$ , is highlighted by yellow solid lines. Equations 2 and 3 summarise the forward pass from the input layer, to hidden layers, and to the output layer:

$$[A]^1 = \sigma([v]^1) = \sigma([\omega]^1 \cdot [P]) \quad \text{Input layer} \quad (2)$$

$$[A]^\ell = \sigma([v]^\ell) = \sigma([\omega]^\ell \cdot [A]^{\ell-1}) \quad \text{Hidden layers} \quad (3)$$

where  $A^x$ ,  $v^x$  and  $\omega^x$  denote the activation, sum-output, and the weight matrices within the  $x^{th}$  layer, respectively. A linear function of output activations forms the predictive action:

$$A_P = f([A]^L) \quad (4)$$

As described in section , upon execution of this action, a series of events take place in the closed-loop platform that leads to the generation of  $E$ , defined in Equation 1; this signal governs the learning of the SaR network.

### The learning goal

The learning goal is to actively and consistently keep the control error at zero; this is achieved through adjusting the

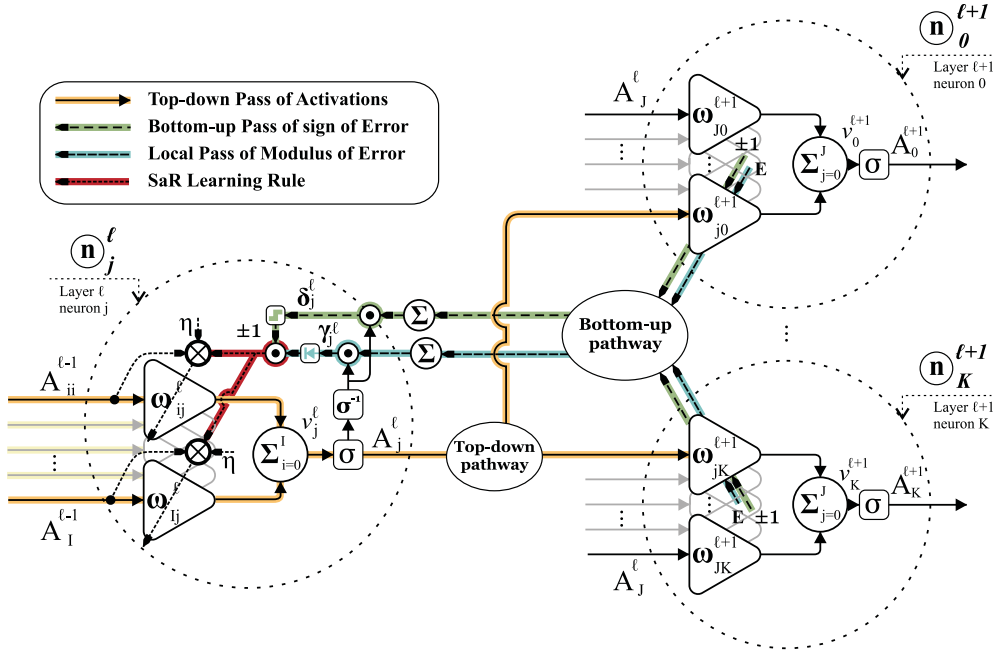


**Figure 3.** Inner connections of neurons in a sign and relevance (SaR) network. Yellow arrows present the forward pass of the activations, green arrows show the bottom-up pass of the sign of error, blue arrows display the local pass of the modulus of error, and red arrows highlight the learning.

weight matrices  $[\omega]^{1 \rightarrow L}$ . From a mathematical standpoint, the learning objective is best formulated as an optimisation task, where the quadratic of the control error is minimised with respect to the weights:

$$[\omega]^{1 \rightarrow L} = \arg \min_{[\omega]} E^2 \quad (5)$$

In other words, we seek weight matrices for all layers, such that the generated action minimises  $E^2$ ; this is analogous to moving  $E$  towards zero. When assigned with an optimisation task, a widely employed practice is that of the gradient descent method (GDM), where the adjustment to an arbitrary weight is proportional to the sensitivity of  $E^2$  with respect to the sum-output of the neuron associated with that weight:

$$\Delta[\omega]^\ell = \frac{\partial E^2}{\partial [v]^\ell} \cdot \frac{\partial [v]^\ell}{\partial [\omega]^\ell} \quad (6)$$

Referring to Equation 3, the later gradient yields the matrix of activation inputs to the neuron:  $[A]^{l-1}$ . The former gradient, however, relates the closed-loop signal ( $E$ ) to an internal parameter of the network ( $v$ ). The linking entity between the closed-loop platform and the neural network is the predictive action  $A_P$  (Daryanavard and Porr 2020), and thus, by applying the chain rule, the closed-loop signals are separated from the internal parameters of the network:

$$\frac{\partial E^2}{\partial [v]^\ell} = \frac{\partial E^2}{\partial A_P} \cdot \frac{\partial A_P}{\partial [v]^\ell} \quad (7)$$

### Dynamics of the closed-loop platform

We seek an expression that relates the control error ( $E$ ) to the predictive output  $A_P$ . In Equation 1, substituting for  $S_a$  results in:

$$\begin{aligned} E &= S_d - \overbrace{Q_R (A_R + A_P + Dz^{-T})}^{\text{Figure 1, node ①}} \\ &= S_d - Q_R (EH_R + A_P + Dz^{-T}) \\ &= \frac{S_d - Q_R (A_P + Dz^{-T})}{1 + Q_R H_R} \end{aligned} \quad (8)$$

Therefore:

$$\kappa = \frac{\partial E^2}{\partial A_P} = 2E \frac{\partial E}{\partial A_P} = 2E \frac{-Q_R}{1 + Q_R H_R} \quad (9)$$

where  $\frac{-Q_R}{1 + Q_R H_R}$  is the reflex loop gain and is measured experimentally. This partial gradient is referred to as the closed-loop gradient and is denoted by  $\kappa$ .

### Inner dynamics of the neural network

We seek an expression that related the predictive output  $A_P$  to the matrix of sum-outputs  $[v]^\ell$  in an arbitrary layer. To that end, Equation 3 can be rewritten as below:

$$\sigma([v]^{\ell+1}) = \sigma([\omega]^{\ell+1} \cdot \sigma([v]^\ell)) \quad (10)$$

Differentiation of  $A_P$  with respect to  $[v]^\ell$  yields:

$$[\delta]_{GDM}^\ell = \frac{\partial A_P}{\partial [v]^\ell} = \sigma^{-1}([v]^\ell) \cdot ([\omega]^{\ell+1})^T \cdot \frac{\partial A_P}{\partial [v]^{\ell+1}} \quad (11)$$

This partial gradient is referred to as the internal error and is denoted by matrix  $[\delta]^\ell$ ; note the recursive nature of this operation, where the calculation of this partial gradient in the  $\ell^{th}$  layer depends on the value of internal error in the  $(\ell + 1)^{th}$  layer. Therefore, starting from the final layer, let  $f$

be the function that generates the predictive output given the activation matrix of the output layer:

$$A_P = f(\sigma([v]^L)) \quad (12)$$

Differentiation with respect to the sum-output matrix in the final layer  $v^L$  yields:

$$[\delta]^L = \frac{\partial A_P}{\partial [v]^L} = f^{-1}(\sigma([v]^L)) \cdot \sigma^{-1}([v]^L) \quad (13)$$

Calculation of internal error in the final layer sets off the bottom-up pass which in turn yields the internal errors for all layers.

### The sign and relevance (SaR) learning rule

In this work, merely the *sign* of the internal error  $[\delta]^\ell$  is used for bottom-up pass into deeper layers, the green dashed arrows in Figure 3 highlight this pathway. The result is a matrix of signs<sup>†</sup> for each layer represented as  $[\pm 1]^\ell$  and calculated as:

$$[\delta]^\ell = \sigma^{-1}([v]^\ell) \cdot ([\omega]^{\ell+1})^T \cdot [\pm 1]^{\ell+1} \quad (14)$$

$$[\pm 1]^\ell = \frac{[\delta]^\ell}{|[\delta]^\ell|} \quad (15)$$

Note that the derivative of the sigmoid function is strictly positive and therefore will have no influence on the resulting sign matrix in Equation 15.

The magnitude of excitation or depression of neurons, however, is derived from a local pass of control error ( $E$ ). This is shown by the blue dashed arrows in Figure 3, and is formulated as:

$$[\gamma]^\ell = \sigma^{-1}([v]^\ell) \cdot ([\omega]^{\ell+1})^T \cdot E \quad (16)$$

where  $[\gamma]^\ell$  is the matrix of local errors in the  $\ell^{th}$  layer. Unlike the internal error, the local error is not passed from deeper layers; meaning that  $[\gamma]^\ell$  does not depend on  $[\gamma]^{\ell+1}$ . Therefore, this signal can be generated simultaneously across all layers globally. For the final layer this is calculated as:

$$[\gamma]^L = f^{-1}(\sigma([v]^L)) \cdot \sigma^{-1}([v]^L) \cdot E \quad (17)$$

With that, the learning rule for the SaR network is defined as:

$$\Delta[\omega]_{\text{SaR}}^\ell = \kappa \cdot \eta \cdot (([\pm 1]^\ell \cdot |[\gamma]^\ell|) \cdot [A]^\ell)^{-1} \quad (18)$$

## Implementation of SaR learning on a navigational robot

The learning algorithm presented in this work is implemented on a path-following robot — the organism, with the task of navigating a canvas whilst retaining a symmetrical positioning on a path printed on the canvas — the environment; see Figure 4C.

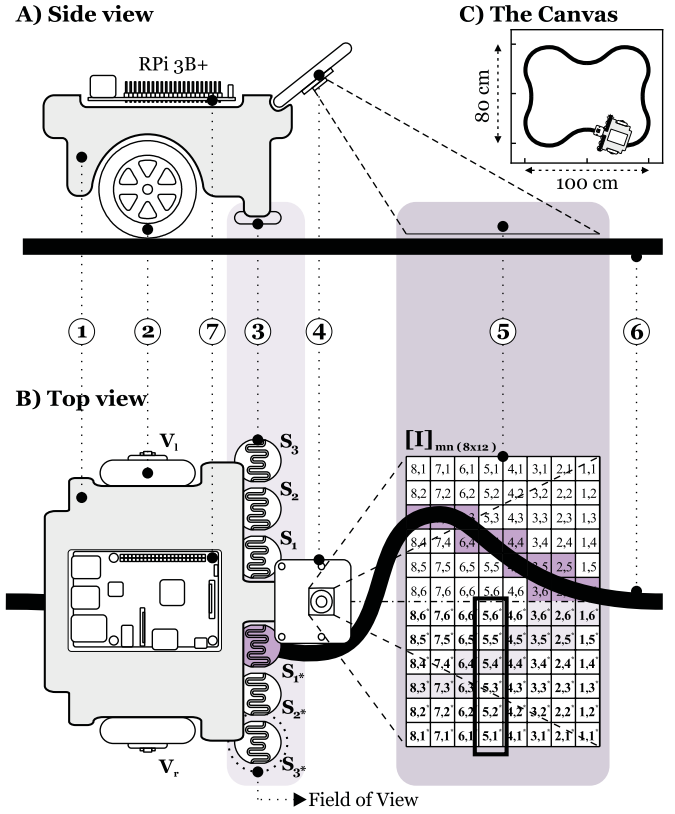


**Figure 4.** Schematics of the navigational robot (not to scale): A) Side view B) Top view; showing the chassis ①, the wheels ②, an array of six light dependent resistors (LDRs) ③, the camera ④, the predictive matrix ⑤, the path ⑥, a Raspberry Pi 3B+ (RPI) ⑦. C) The canvas and the path.

### The robotic platform

Schematic drawings of the robot are shown in Figure 4 (not to scale). The chassis of the robot houses a battery and contains the wiring of the components. The robot consists of two wheels, an array of light sensors and a camera. The camera provides a vision of the path ahead in the form of a matrix. A Raspberry Pi 3B+ (RPI) with a remote connection is used as a processing centre that hosts the SaR algorithm. In the following subsections, both reflex and predictive sensory inputs, as well as the motor command, are described and the components of the robot are discussed in depth.

### Reflex sensory inputs

The light array consists of 6 symmetrically positioned light dependent resistors (LDRs) which are placed underneath the chassis in close proximity to the canvas, as in Figure 4A, labelled  $S_{1,2,3}$  on the left and  $S_{1^*,2^*,3^*}$  on the right<sup>‡</sup> side of the robot, as in Figure 4B. Each sensor receives the reflected light from a small portion of the canvas directly underneath. This region is referred to as the field of view (FoV) of the sensor, which is indicated by a dotted circle around sensor  $S_{3^*}$  in Figure 4B. During navigation, these sensors translate the changes in the intensity of the reflected light into voltage fluctuations. As the FoV of a sensor transitions

<sup>†</sup>This matrix only contains values of +1, -1 or 0.

<sup>‡</sup>The star sign indicates the symmetrical positioning of an arbitrary sensor with respect to its unmarked counterpart

from capturing the black path entirely to capturing the white background, it generates a voltage potential within the range of  $(600 - 1500)[mV]$ . The grey value (G),  $G_i$  or  $G_{i^*}$ , of each sensor is found through a linear mapping of their voltage potentials to the range  $[0, 256] \in \mathbb{N}$  to represent the grey-scale value (GSV) of their respective FoVs. The grey value of each sensor is proportional to the presence of the black path in their FoV which provides a measure of the vertical alignment of the sensor with respect to the path and thus serves as an indicator for the relative positioning of the robot. For example, sensor  $S_{1^*}$  in Figure 4B is vertically aligned with the path indicating a slight overall deviation of the robot to the left, whereas, the alignment of sensor  $S_3$  would indicate a significant overall deviation to the right.

In technical terms, the deviation of the robot from the path is measured through a weighted sum of differences in grey values of sensor pairs. Thus, the experimental value of the control error ( $E$ ), previously defined in Equation 1, is found as:

$$E = \sum_{i=1}^3 K_i (G_i - G_{i^*}) \quad [\text{GSV}] \quad (19)$$

where  $K_i$  is a weighting factor whose magnitude increases linearly with  $i$ , to reflect the degree of deviation. Meaning that the farther the active sensor from the centreline the greater the spike in  $E$ , indicating a greater deviation.

### Predictive sensory inputs

the camera provides information about the path in the near distance and thus facilitates anticipatory steering of the robot. The camera captures a 1280 by 720 pixel image which is segmented into regions as in Figure 4B. Each square region is assigned the average GSVs of the pixels it contains. This generates the sensory input from the camera in the form of a 8 by 12 matrix  $[I]_{mn}$ . Similar to that of the light array sensors, the difference of symmetrical entries in this matrix measures the anticipated degree of deviation in the near distance:

$$C_{ij} = I_{ij} - I_{ij^*} \quad (20)$$

$$\text{where } 1 \leq i \leq m, \quad 1 \leq j \leq \lfloor \frac{n}{2} \rfloor \quad \text{and} \quad j^* + j = n + 1$$

Where  $C_{ij}$  are the camera signals that form an 8 by 6 matrix. A non-zero  $C_{ij}$  indicates an upcoming turn; the value of  $j$  indicates the sharpness of the turn, whilst the value of  $i$  indicates the distance of the turn from the current position, and the sign of  $C_{ij}$  indicates a right or left turn. Each difference signal is delayed using a filter array (FA) of 5 finite impulse response (FIR) filters,  $F_h$ , to observe an optimum correlation with the control error signal for learning (Daryanavard and Porr 2020):

$$P_k = F_h * C_{ij} \quad (21)$$

$$\text{where } 1 \leq h \leq 5, \quad 1 \leq i \leq m, \quad 1 \leq j \leq \lfloor \frac{n}{2} \rfloor$$

This results in a sequence of 240 predictor signals  $P_k$  which are fed into the SaR network for prediction and producing anticipatory actions.

### The motor command (MC)

The navigation of the robot is facilitated through adjustments to the speed of the right and left wheels,  $V_R$  and  $V_L$ , that otherwise proceed forward with a fixed speed of  $V_0 = 5[\frac{cm}{s}]$ . A motor command (MC) is sent to the wheels to modify their velocities as:

$$\begin{cases} V_R = V_0 + MC, & \text{for right wheel.} \\ V_L = V_0 - MC, & \text{for left wheel.} \end{cases} \quad (22)$$

MC is generated jointly by both the reflex and predictive mechanism of the robot and hence is the sum of reflex and predictive actions introduced in Section :

$$MC = A_R + A_P \quad (23)$$

where  $A_R$  is proportional to  $E$  and  $A_P$  is a weighted sum of the activations in the output layer as indicated in Equation 12:

$$\begin{cases} A_R \propto E, & \text{reflex action.} \\ A_P = f([A]^L) = [M] \cdot [A]^L, & \text{predictive action.} \end{cases} \quad (24)$$

where  $[M]$  is a weighting matrix for output activations; this facilitates sharp, moderate, or slow steering of the robot depending on the active neuron and its weight factor. At the initial stages of a trial,  $A_R$  is the main contributor to the motor command, as the learning progresses  $A_P$  delivers a more adequate contribution, and upon successful learning, where the SaR network has generated the forward model of the reflex,  $A_R$  is kept at zero at all times and  $A_P$  alone controls the motor command.

### The architecture of the sign and relevance (SaR) network

This application employs a feed-forward neural network with fully-connected layers. As derived in Equation 21, there are 240 inputs from the camera, and thus, the network is initialised with 240 neurons in the input layer. The number of neurons in the hidden layers decrements linearly from 13 to 4 through 10 hidden layers in an encoder style funnel. Finally, there are 3 neurons in the output layer and the weighted sum of their activations, using  $[M] = [1, 3, 5]$ , yields the predictive action as in Equation 24.

## Results

In this section, we present a comparison between the conventional GDM technique and SaR learning. The GDM learning rule is conventionally defined as:

$$\Delta[\omega]_{GDM}^\ell = \kappa \cdot \eta \cdot ([\beta]^\ell \cdot [A]^{\ell-1}) \quad (25)$$

where  $\beta$  is calculated similarly to Equation 14:

$$[\beta]^\ell = \sigma^{-1}([v]^\ell) \cdot ([\omega]^{\ell+1T} \cdot [\beta]^{\ell+1}) \quad (26)$$

Figure 5 shows a set of trials with a learning rate of  $\eta = e^{-5}$ . Panels A and B show the control error ( $E$ ) signal (solid traces) and its absolute moving average over 25 seconds:  $\bar{E} = \int_t^{t-25} |E(t)|$  (dashed traces) for the two

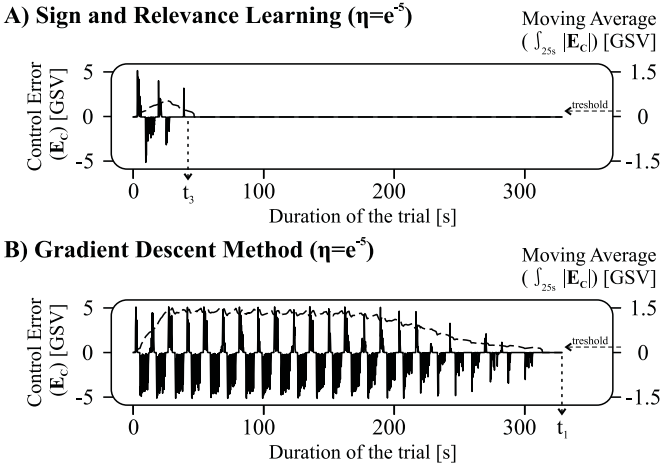


**Figure 5.** The control error ( $E$ ) signal and its 25[s] moving average during learning trials with SaR learning (A) and conventional GDM (B) with the learning rate of  $\eta = e^{-5}$ .

learning modalities mentioned above. We define *success* as a state where  $\bar{E}$  falls below a value of 0.1[GSV] (left-hand-side axes); this is evaluated 12 seconds after the trial has commenced allowing for the signal to accumulate.

During a trial with GDM (panel B), the error signal is persistent for approximately 200 seconds before it gradually converges reaching the success state at time  $t_1 = 333[s]$ . This trial sets a benchmark for the evaluation of SaR paradigm. Panel A shows these results for a trial with SaR learning, where the bottom-up pass of the sign of the error, and the magnitude of the locally passed error, join to drive the weight changes. It can be seen that the learning is significantly improved, in that, the error signal does not persist, rather, it immediately begins to converge and successful learning is achieved at time  $t_3 = 42[s]$ .

Figure 6 shows another set of trials with a faster learning rate of  $\eta = e^{-1}$ . In panel B, during a trial with GDM, the error signal spikes over a period of 25[s] before it fully converges at  $t_4 = 32[s]$ . In panel A, *one-shot* learning is achieved during a trial with SaR; the error signal spikes once at  $t = 5[s]$  and the success state is achieved at  $t = 12[s]$ . It can be seen that in this trial the moving average remains below the success threshold, therefore total integral of the error is a better comparative factor which will be presented in Figure 10.

Additional information about another one-shot learning trial with SaR is presented in Figure 7. Panels A, B and C show the control error signal, the activity of six selected predictive signals marked with a rectangle in Figure 4B, and the predictive action  $A_P$ , respectively. The robot first encounters the line at time  $t_7 = 8[s]$ . Prior to this instant, some predictive signals are active (non-zero), however, there is no steering signal at the output of the network ( $A_P = 0$ )<sup>§</sup>. Upon encountering the line, the control error spikes. This signal generates the reflex reaction to return the robot to the path and trains the neural network to produce adequate steering signals. Hence, the error signal returns to zero at  $t_8 = 9[s]$ . The gradual increase in the output of the network from  $t_7$  to  $t_8$ , in panel C, signifies the learning driven by the non-zero error signal during this interval. Subsequent to this learning, the predictive signals provide the network

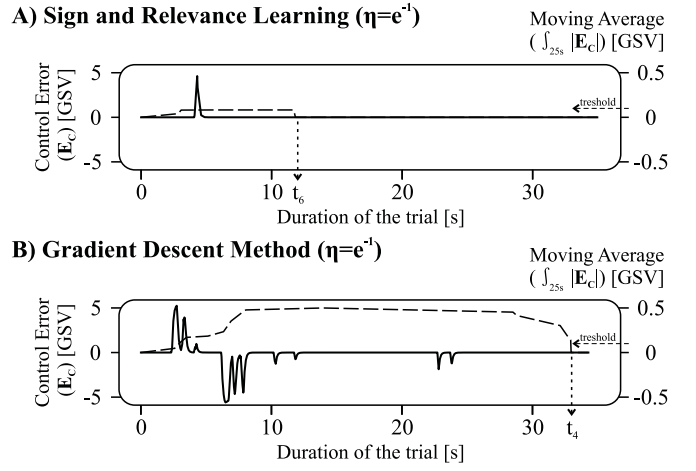


**Figure 6.** The control error ( $E$ ) signal and its 25[s] moving average during learning trials with SaR learning (A) and conventional GDM (B) with the learning rate of  $\eta = e^{-1}$ .

with clues about the path ahead which produces adequate predictive action, as a result, the error signal remains at zero for the remainder of this trial.

Naturally, one-shot learning in the context of deep learning begs the question of weight stability. In this work, the Euclidean distance of weights in each layer is used as an indicator of weight convergence stability. This is calculated as the multidimensional distance of the weight matrix  $[\omega]$  at time  $t'$  from its initialisation matrix at time  $t_0$ :

$$Ed(t') = Euclidean([\omega]_{t'}, [\omega]_{init}) \quad (27)$$

$$= \sqrt{\sum_{i,j=0}^{I,J} (\omega_{ij}^{\ell}|_{t'} - \omega_{ij}^{\ell}|_{t_0})^2}$$

<sup>§</sup>This is because the robot is initially positioned on the path symmetrically.

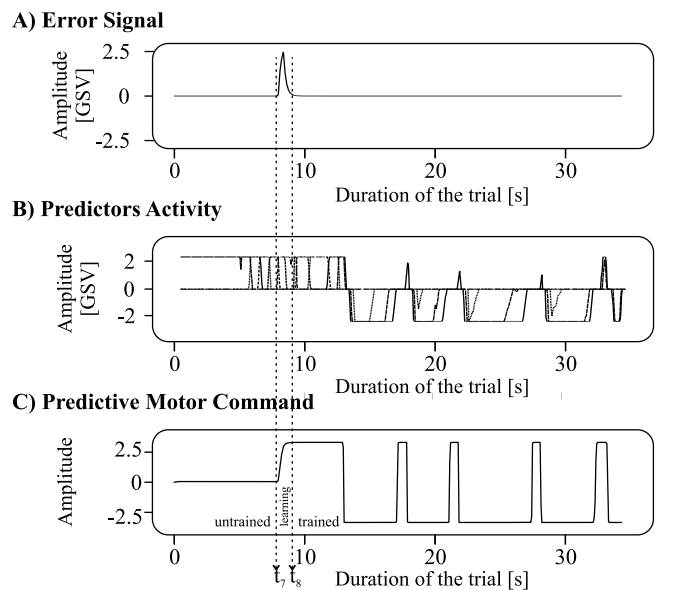


**Figure 7.** The control error ( $E$ ) signal (A), the activity of six selected predictive signals (B), and the output of the neural network (C) during a learning trial with SaR learning with the learning rate of  $\eta = e^{-1}$ .

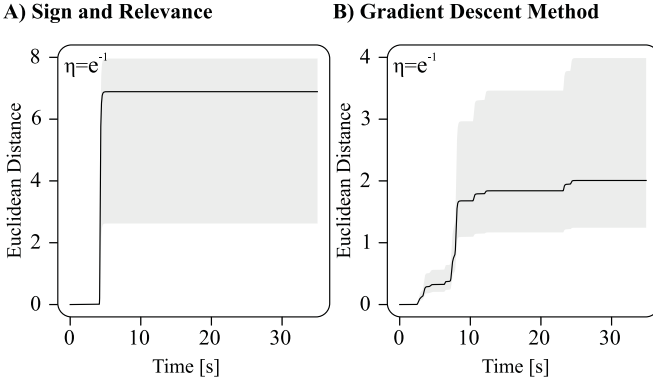


**Figure 8.** The Euclidean distance of weights in the first layer (black traces) and in deeper layers (grey shadow) during learning trials with SaR learning (A), conventional GDM (B), with the learning rate of  $\eta = e^{-1}$ .

This parameter is calculated within individual layers of the network where  $\ell$  is constant.

Figure 8 shows the Euclidean distance of weights during the three trials previously produced in Figure 5. Panel B shows that in a trial with GDM, the final Euclidean distances of weights in deeper layers fall within a range of 1.2 to 4 (the grey area). However, the changes in the first layer, where the sensory consequences of motor actions are perceived, carry more significance (Porr and Miller 2020). Therefore, the Euclidean distance of the first layer is shown individually by the black trace with a final distance of  $\approx 2$  for this trial. Panel A shows this result for a trial with SaR learning where the Euclidean distance is moderately greater than that of the GDM, with final distances of 3 to 8 for deeper layers and  $\approx 7$  for the first layer. Though the Euclidean distance has almost doubled, it has done so whilst improving the speed and the performance of the SaR learner.

As mentioned above, there is a greater significance associated with the first hidden layer where the organism learns to assign importance to the sensory inputs received from the environment. Figure 9 displays the final weight distributions in the first hidden layer for the trials previously discussed in Figures 5 and 8. There are 240 predictive input signals and 13 neurons in the first hidden layer, making a weight matrix of size 240 by 13. The values in this matrix are normalised to the range of  $[0, 1]$  and are assigned a grey shade, with white corresponding to 0 and black to 1, creating an image of weight distribution. Common observations amongst the two learning paradigms are: 1) the 8 rows of predictors (see Figure 4) are appropriately classified into recognisable blocks, 2) within each block there is a gradient where the outermost columns of predictors (see Figure 4) are assigned a higher value producing sharper steering and, 3) this gradient is more predominant for rows of predictors closer to the robot (rightmost blocks). However, a comparison of the trials reveals a more assured and well-defined gradient for SaR learning (panel A) than that of the GDM (panel B).

The trials presented in Figure 5 were repeated 10 times to demonstrate the reproducibility of the results. Figures 10 A and B display the total error integral and the time taken to reach the success condition for trials with SaR and GDM learning. In support of the results produced in Figure 5,

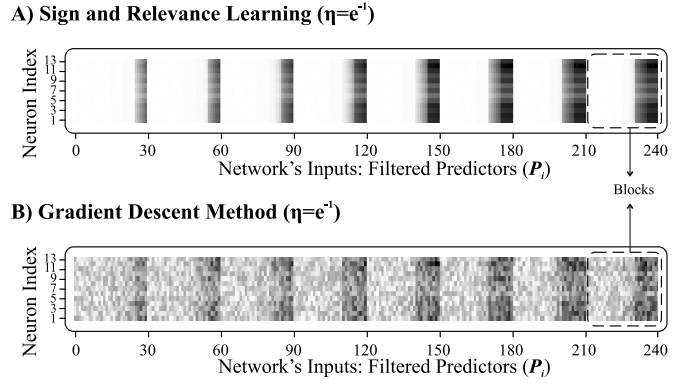


**Figure 9.** Final weight distributions in the first hidden layer during learning trials with SaR learning (A), and conventional GDM (B), with the learning rate of  $\eta = e^{-1}$ .

it can be concluded that SaR consistently provides faster learning with smaller error accumulation. Additional trials were carried out with SaR learning only with learning rates of  $\eta = \{e^{-5}, e^{-4}, e^{-3}, e^{-2}, e^{-1}\}$ ; Figure 11 shows the result of these experiments.

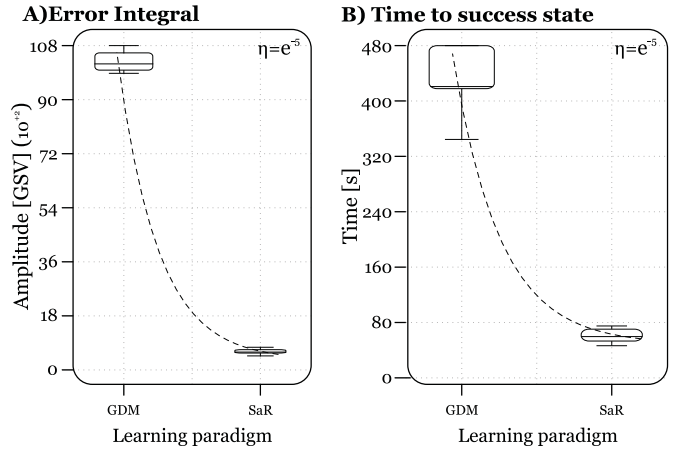


**Figure 10.** Reproducibility of results showing total error integral (A) and time taken to success state (B) for 10 trials with GDM and SaR learning.

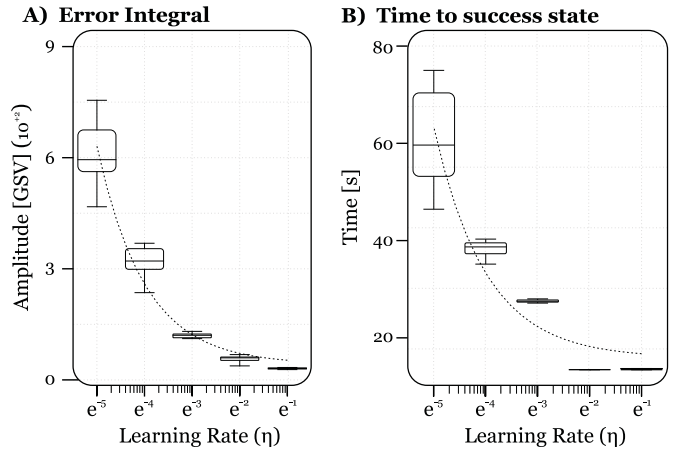


**Figure 11.** Reproducibility of results with different learning rates showing total error integral (A) and time taken to success state (B) for trials SaR learning.

## Discussion

In this paper, we presented a learning algorithm that separates the error signal into a global and local component where its sign is passed in a bottom-up fashion through the network while its rectified value is transmitted globally to all layers. In contrast to classical back-propagation, this approach is significantly faster in a closed-loop learning task and complies with neurophysiology more closely by employing both neuromodulators and local learning rules while not requiring strictly symmetric weights.

Deep learning has become very popular over the last decade (Guo et al. 2014) and given that it uses neural networks it should also be a good candidate to explain how the brain itself conducts learning (Marblestone et al. 2016). For example, Lillicrap et al. (2016) maps deep learning on the brain, however, due to the neurophysiologically unrealistic requirement of symmetric weights between forward and backward pathways this is limited to a few layers.

On the other hand, traditional biologically realistic reinforcement learning models (Schultz and Suri 2001; Wörgötter and Porr 2005; Prescott et al. 2006) employ the reward prediction error which has a strong familiarity to the dopaminergic signal in the striatum (Schultz et al. 1997). These models are certainly closer to biology but suffer from the problem that any global error signal poses for deep structures namely, the different layers change all similarly and therefore a deep structure adds little to their performance.

However, do reward-related neuromodulators convey error signals as it has been the dominant paradigm during the last two decades Schultz et al. (1997)? Serotonin appears to rather code reward expectation (Li et al. 2016) which could at best be called a “rectified” reward prediction error. Similarly, the negative response of dopamine neurons to a negative reward expectation has been declared unreliable by Schultz (2004) due to its low baseline firing rate of approximately 1 Hz, resulting in a very low signal-to-noise ratio. A different interpretation for both the serotonin and also the dopamine signal is that of a relevance signal (Porr and Wörgötter 2007) ramping up or enabling plasticity (Loving 2010; Iigaya et al. 2018) while local plasticity learning rules determine if synaptic weights undergo long-term potentiation (LTP) or long-term depression (LTD) (Castellani et al. 2001; Inglebert et al. 2020).

Given that we have established global and local learning we can now discuss how such processing can be established in a biologically realistic fashion. Figure 12 shows the suggested circuit inspired by Larkum (2013); Rolls (2016) and with added neuromodulatory innervation (Loving 2010; Iigaya et al. 2018). This circuit has two distinct pathways where the top-down pathway carries, for example, sensor signals to deeper structures of the brain or directly to motor outputs. As an example, a single top-down path is depicted from “In” to “Out” via three synapses connecting the three neurons in layer zero (L0) to layer two (L2). Having described the top-down path, we can now consider the bottom-up path. It transmits the sign of the error signal from layer two back to layer zero; this pathway also has three synapses. Finally, notice the global neuromodulation

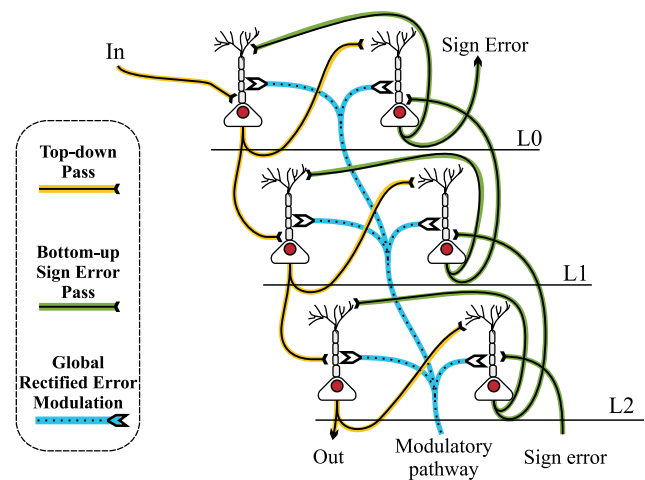


**Figure 12.** Proposal of a neurophysiologically realistic model of SaR learning. Shown are three network layers L0, L1 and L2. Signal processing is performed in three pathways: “Top-down” which transmits a signal from “In” to “Out”, a “Bottom-up” pathway which transmits the Sign error and a “Modulatory pathway” which provides a global signal to all neurons. The top-down and bottom-up pathways transmit signals via synapses close to the respective somas while the reciprocal connections between the neurons within a layer connect to the dendrites influencing plasticity.

which controls the plasticity of all neurons; this leads us to the plasticity rules. Central to this circuit is that the local plasticity is driven by the concentration of postsynaptic Calcium. Following the reasoning of Inglebert et al. (2020), only a strong Calcium influx caused by both somatic burst spiking and dendritic Calcium spikes will lead to long-term potentiation (LTP) while less activity, in particular lack of dendritic Calcium bursts, will lead to long-term depression (LTD). Projections from the distal parts to the dendrite are not able to make the neuron spike, however, if coincident with a somatic input, it will create long-lasting bursting causing LTP (Larkum 2013) owing to a large influx of Calcium (Inglebert et al. 2020). Conversely, if the dendritic trees are not sufficiently driven, LTD will be initiated due to a smaller Calcium influx from single spikes (Inglebert et al. 2020; Shouval et al. 2002). Thus, the sign of the weight development between reciprocal neurons, within a layer in both top-down and bottom-up pathways, is mirrored due to their reciprocal connections and their ability to boost or deprive each other’s Calcium concentrations. The neuromodulator then controls the learning rate. Future research is needed to investigate this model in depth using more detailed biophysical modelling to carry positive implications, for example, for mental illness models (Rolls 2016).

## Declaration of conflicting interests

There is no conflict of interest in this work.

## Funding

We would like to thank Engineering and Physical Sciences Research Council (EPSRC) division of UK Research and Innovation (UKRI) for funding (EP/N509668/1 and EP/R513222/1) this project.

## Acknowledgements

We would like to acknowledge Jarez Patel for his valuable intellectual and technical input for the making of the robotic platform.

## References

- Berthoud H (2004) Mind versus metabolism in the control of food intake and energy balance. *Physiol Behav* 81(5): 781–793.
- Bliss T and Lomo T (1973) Long-lasting potentiation of synaptic transmission in the dentate area of the anaesthetized rabbit following stimulation of the perforant path. *J Physiol* 232(2): 331–356.
- Bromberg-Martin ES, Matsumoto M and Hikosaka O (2010) Dopamine in motivational control: rewarding, aversive, and alerting. *Neuron* 68(5): 815–34. DOI:10.1016/j.neuron.2010.11.022.
- Castellani GC, Quinlan EM, Cooper LN and Shouval HZ (2001) A biophysical model of bidirectional synaptic plasticity: Dependence on AMPA and NMDA receptors. *Proc. Natl. Acad. Sci. (USA)* 98(22): 12772–12777.
- Daryanavard S and Porr B (2020) Closed-loop deep learning: Generating forward models with backpropagation. *Neural Computation* 32(11): 2122–2144.
- Dayan P and Balleine BW (2002) Reward, motivation, and reinforcement learning. *Neuron* 36(2): 285–298.
- Guo X, Singh S, Lee H, Lewis RL and Wang X (2014) Deep learning for real-time atari game play using offline monte-carlo tree search planning. In: Ghahramani Z, Welling M, Cortes C, Lawrence ND and Weinberger KQ (eds.) *Advances in Neural Information Processing Systems* 27. Curran Associates, Inc., pp. 3338–3346.
- Haber S, Kunishio K, Mizobuchi M and Lynd-Balta E (1995) The orbital and medial prefrontal circuit through the primate basal ganglia. *J Neurosci* 15(7 Pt 1): 4851–4867.
- Hebb DO (1949) *The organization of behavior: A neuropsychological study*. New York: Wiley-Interscience.
- Humphries MD, Stewart RD and Gurney KN (2006) A physiologically plausible model of action selection and oscillatory activity in the basal ganglia. *Journal of Neuroscience* 26(50): 12921–12942. DOI:10.1523/JNEUROSCI.3486-06.2006. URL <https://www.jneurosci.org/content/26/50/12921>.
- Iigaya K, Fonseca MS, Murakami M, Mainen ZF and Dayan P (2018) An effect of serotonergic stimulation on learning rates for rewards apparent after long intertrial intervals. *Nature Communications* 9(1): 2477. DOI:10.1038/s41467-018-04840-2. URL <https://doi.org/10.1038/s41467-018-04840-2>.
- Inglebert Y, Aljadeff J, Brunel N and Debanne D (2020) Synaptic plasticity rules with physiological calcium levels. *Proc Natl Acad Sci U S A* 117(52): 33639–33648. DOI:10.1073/pnas.2013663117.
- Larkum M (2013) A cellular mechanism for cortical associations: an organizing principle for the cerebral cortex. *Trends in neurosciences* 36(3): 141–151.
- Li Y, Zhong W, Wang D, Feng Q, Liu Z, Zhou J, Jia C, Hu F, Zeng J, Guo Q, Fu L and Luo M (2016) Serotonin neurons in the dorsal raphe nucleus encode reward signals. *Nature Communications* 7(1): 10503. DOI:10.1038/ncomms10503. URL <https://doi.org/10.1038/ncomms10503>.
- Lillicrap TP, Cownden D, Tweed DB and Akerman CJ (2016) Random synaptic feedback weights support error backpropagation for deep learning. *Nature communications* 7: 13276. DOI:10.1038/ncomms13276.
- Linley SB, Hoover WB and Vertes RP (2013) Pattern of distribution of serotonergic fibers to the orbitomedial and insular cortex in the rat. *Journal of chemical neuroanatomy* 48–49: 29–45. DOI:10.1016/j.jchemneu.2012.12.006. URL <http://www.ncbi.nlm.nih.gov/pubmed/23337940>.
- Lovinger DM (2010) Neurotransmitter roles in synaptic modulation, plasticity and learning in the dorsal striatum. *Neuropharmacology* 58(7): 951–61. DOI:10.1016/j.neuropharm.2010.01.008.
- Lu W, Man H, Ju W, Trimble WS, MacDonald JF and Wang YT (2001) Activation of synaptic NMDA receptors induces membrane insertion of new AMPA receptors and LTP in cultured hippocampal neurons. *Neuron* 29(1): 243–54. DOI: 10.1016/S0896-6273(01)00194-5.
- Luo M, Zhou J and Liu Z (2015) Reward processing by the dorsal raphe nucleus: 5-HT and beyond. *Learn Mem* 22(9): 452–60. DOI:10.1101/lm.037317.114.
- Maffei G, Herreros I, Sanchez-Fibla M, Friston KJ and Verschure PF (2017) The perceptual shaping of anticipatory actions. *Proceedings of the Royal Society B: Biological Sciences* 284(1869): 20171780.
- Marblestone AH, Wayne G and Körding KP (2016) Toward an integration of deep learning and neuroscience. *Frontiers in computational neuroscience* 10: 94.
- Markram H, Lübke J, Frotscher M and Sakman B (1997) Regulation of synaptic efficacy by coincidence of postsynaptic apss and epsps. *Science* 275: 213–215.
- Mattson MP, Maudsley S and Martin B (2004) Bdnf and 5-HT: a dynamic duo in age-related neuronal plasticity and neurodegenerative disorders. *Trends in Neurosciences* 27(10): 589–594. DOI:https://doi.org/10.1016/j.tins.2004.08.001. URL <https://www.sciencedirect.com/science/article/pii/S0969996104000594>.
- O'Reilly RC and Frank MJ (2006) Making Working Memory Work: A Computational Model of Learning in the Prefrontal Cortex and Basal Ganglia. *Neural Computation* 18(2): 283–328. DOI:10.1162/089976606775093909. URL <https://doi.org/10.1162/089976606775093909>.
- Porr B and Miller P (2020) Forward propagation closed loop learning. *Adaptive Behavior* 28(3): 181–194.
- Porr B and Wörgötter F (2003) Isotropic-sequence-order learning in a closed-loop behavioural system. *Philosophical Transactions of the Royal Society of London A: Mathematical, Physical and Engineering Sciences* 361(1811): 2225–2244.
- Porr B and Wörgötter F (2006) Strongly improved stability and faster convergence of temporal sequence learning by using input correlations only. *Neural computation* 18(6): 1380–1412.
- Porr B and Wörgötter P (2002) Isotropic sequence order learning using a novel linear algorithm in a closed loop behavioural system. *Biosystems* 67(1–3): 195–202.
- Porr B and Wörgötter F (2007) Learning with “Relevance”: Using a Third Factor to Stabilize Hebbian Learning. *Neural Computation* 19(10): 2694–2719. DOI:10.1162/neco.2007.19.10.2694. URL <https://doi.org/10.1162/neco.2007.19.10.2694>.
- Prescott TJ, González FMM, Gurney K, Humphries MD and Redgrave P (2006) A robot model of the basal ganglia: behavior

- and intrinsic processing. *Neural networks* 19(1): 31–61.
- Roberts AC (2011) The importance of serotonin for orbitofrontal function. *Biol. Psychiatry* 69(12): 1185–91. DOI:10.1016/j.biopsych.2010.12.037.
- Rolls ET (2016) Reward systems in the brain and nutrition. *Annual review of nutrition* 36: 435–470.
- Rolls ET and Grabenhorst F (2008) The orbitofrontal cortex and beyond: From affect to decision-making. *Progress in Neurobiology* 86(3): 216–244. DOI: <https://doi.org/10.1016/j.pneurobio.2008.09.001>. URL <https://www.sciencedirect.com/science/article/pii/S0301008208000981>.
- Schultz W (2004) Neural coding of basic reward terms of animal learning theory, game theory, microeconomics and behavioural ecology. *Curr Opin Neurobiol* 14(2): 139–147.
- Schultz W, Dayan P and Montague PR (1997) A neural substrate of prediction and reward. *Science* 275: 1593–1599.
- Schultz W and Suri RE (2001) Temporal difference model reproduces anticipatory neural activity. *Neural Comp.* 13(4): 841–862.
- Shouval HZ, Bear MF and Cooper LN (2002) A unified model of NMDA receptor-dependent bidirectional synaptic plasticity. *Proc. Natl. Acad. Sci. (USA)* 99(16): 10831–10836.
- Sutton R (1988) Learning to predict by method of temporal differences. *Machine Learning* 3(1): 9–44.
- Takahashi YK, Batchelor HM, Liu B, Khanna A, Morales M and Schoenbaum G (2017) Dopamine neurons respond to errors in the prediction of sensory features of expected rewards. *Neuron* 95(6): 1395–1405.e3. DOI:<https://doi.org/10.1016/j.neuron.2017.08.025>. URL <https://www.sciencedirect.com/science/article/pii/S0896627317307407>.
- Verschure PF and Coolen AC (1991) Adaptive fields: Distributed representations of classically conditioned associations. *Network: Computation in Neural Systems* 2(2): 189–206.
- von Uexküll BJJ (1926) *Theoretical biology*. London: Kegan Paul, Trubner.
- Wood J, Simon NW, Koerner FS, Kass RE and Moghaddam B (2017) Networks of VTA Neurons Encode Real-Time Information about Uncertain Numbers of Actions Executed to Earn a Reward. *Front Behav Neurosci* 11: 140. DOI: 10.3389/fnbeh.2017.00140.
- Wörgötter F and Porr B (2005) Temporal sequence learning, prediction and control - a review of different models and their relation to biological mechanisms. *Neural Comp* 17: 245–319.